Title of article: Role of Cytosolic, Tyrosine-Insensitive Prephenate Dehydrogenase in *Medicago truncatula*

Authors: Craig A. Schenck[1,2], Josh Westphal[1], Dhileepkumar Jayaraman[3], Kevin Garcia[3,4], Jiangqi Wen[5], Kirankumar S. Mysore[5] Jean-Michel Ané[3,6], Lloyd W. Sumner[7,8] and Hiroshi A. Maeda[1,*]

Affiliations: [1]Department of Botany, University of Wisconsin-Madison, Madison, WI 53706
[2] Current address: Department of Biochemistry and Molecular Biology, Michigan State University, East Lansing, MI 48824
[3] Department of Bacteriology, University of Wisconsin-Madison, Madison, WI 53706
[4] Department of Crop and Soil Sciences, North Carolina State University, Raleigh, NC 27695
[5] Noble Research Institute, LLC., Ardmore, OK, USA
[6] Department of Agronomy, University of Wisconsin-Madison, Madison, WI 53706
[7] Department of Biochemistry, University of Missouri, Columbia, MO 65211
[8] Metabolomics and Bond Life Sciences Centers, University of Missouri, Colubmia, MO 65211

[*]Corresponding author: Hiroshi A. Maeda (maeda2@wisc.edu)

ABSTRACT

L-Tyrosine (Tyr) is an aromatic amino acid synthesized *de novo* in plants and microbes downstream of the shikimate pathway. In plants, Tyr and a Tyr pathway intermediate, 4-hydroxyphenylpyruvate (HPP), are precursors to numerous specialized metabolites, which are crucial for plant and human health. Tyr is synthesized in the plastids by a TyrA family enzyme, arogenate dehydrogenase (ADH/TyrA$_a$), which is feedback inhibited by Tyr. In addition to ADH enzymes, many legumes possess prephenate dehydrogenases (PDH/TyrA$_p$), which are insensitive to Tyr and localized to the cytosol. Yet the role of PDH in legumes is currently unknown. This study isolated and characterized *Tnt1*-transposon mutants of *MtPDH1* (*pdh1*) in *Medicago truncatula* to investigate PDH function. The *pdh1* mutants lacked *PDH* transcript, PDH activity, and displayed little aberrant morphological phenotypes under standard growth conditions providing genetic evidence that *MtPDH1* is responsible for the PDH activity detected in *M. truncatula*. Though plant PDH enzymes and activity have been specifically found in legumes, nodule number and nitrogenase activity of *pdh1* mutants were not significantly reduced compared to wild-type (Wt) during symbiosis with nitrogen-fixing bacteria. Although Tyr levels were not significantly different between Wt and mutants under standard conditions, when carbon flux was increased by shikimate precursor feeding, mutants accumulated significantly less Tyr than Wt. These data suggest that MtPDH1 is involved in Tyr biosynthesis when the shikimate pathway is stimulated, and possibly linked to unidentified legume-specific specialized metabolism.

INTRODUCTION

L-Tyrosine (Tyr) is an aromatic amino acid synthesized *de novo* in plants and microbes, but not animals; thus, humans must acquire Tyr through their diet or by enzymatic conversion of L-phenylalanine (Phe, Fitzpatrick, 1999). In addition to its involvement in protein synthesis, Tyr and a Tyr-pathway intermediate 4-hydroxyphenylpyruvate (HPP) are the precursors to numerous specialized metabolites crucial for plant and animal health (Schenck and Maeda, 2018). Tyr-derived plant specialized metabolites have roles as photosynthetic electron carriers (plastoquinone, Metz et al., 1989), pollinator attractors (betalain pigments, Strack et al., 2003) and in defense (dhurrin and rosmarinic acid, Møller, 2010; Petersen, 2013). In grasses, Tyr also serves as a precursor to lignin, the main structural polymer in plants (Higuchi et al., 1967; Rosler et al., 1997; Barros et al., 2016). Humans have co-opted some of these natural products to serve nutritional and medicinal roles such as some benzylisoquinoline alkaloids, which have antitussive, analgesic, and antimicrobial activities (Barken et al., 2008; Beaudoin and Facchini, 2014; Kries and O'Connor, 2016), and the antioxidant properties of tocopherols (collectively referred to as vitamin E, Bramley et al., 2000).

The aromatic amino acids (AAAs; Tyr, Phe, and tryptophan [Trp]) are synthesized in the plastids from chorismate, the final product of the shikimate pathway (Tzin and Galili, 2010; Maeda and Dudareva, 2012). Chorismate mutase (CM, EC number 5.4.99.5) catalyzes the committed step of Tyr and Phe synthesis — the isomerization of chorismate into prephenate (Goers and Jensen, 1984; Kuroki and Conn, 1989; Eberhard et al., 1996; Mobley et al., 1999). Prephenate is converted to Tyr via two reactions, oxidative decarboxylation catalyzed by a TyrA dehydrogenase enzyme and transamination. These reactions can occur in either order, leading to alternative Tyr pathways (**Fig. 1**, Schenck and Maeda, 2018). In most microbes, a prephenate-specific TyrA dehydrogenase (PDH/TyrA$_p$ EC 1.3.1.13, **Fig. 1**) first converts

prephenate into HPP followed by transamination to Tyr via Tyr-aminotransferase (Tyr-AT or TyrB, EC2.6.1.5). In plants, these reactions occur in the reverse order with transamination of prephenate to form arogenate by a plastidic prephenate aminotransferase (PPA-AT, EC 2.6.1.78), followed by oxidative decarboxylation catalyzed by a plastidic arogenate-specific TyrA dehydrogenase (ADH/$TyrA_a$ EC 1.3.1.78) producing Tyr (**Fig. 1**). The ADH-mediated Tyr pathway appears to be essential for normal growth and development in plants as indicated by the severe phenotype of *Arabidopsis thaliana adh2/tyra2* knockout mutant, which was further exacerbated by transient suppression of the other *ADH1/TyrA1* gene (de Oliveira et al., 2019). PDH and ADH are the key enzymes in their respective pathways, as they compete for substrates that are shared with Phe biosynthesis, and are generally feedback inhibited by Tyr (Rubin and Jensen, 1979; Gaines et al., 1982; Connelly and Conn, 1986; Rippert and Matringe, 2002).

PDH activity, which is commonly found in microbes, has been detected in tissue extracts of some plants, all restricted to the legume family (Gamborg and Keeley, 1966; Rubin and Jensen, 1979; Siehl, 1999). In soybean, leaf tissue had the highest PDH activity of all analyzed tissues (Schenck et al., 2015). Phylogenetic analyses of plant and microbial TyrAs showed that *PDH* genes are uniquely present in legumes, suggesting that legume PDH enzymes are the result of a recent legume-specific gene duplication event of a plant *ADH* rather than horizontal gene transfer from a *PDH*-possessing rhizobia (Schenck et al., 2015). However, not all legumes possess *PDH*, which suggests gene loss in some legumes (Schenck et al., 2015; Schenck et al., 2017a). PDH recombinant enzymes from *Glycine max* (soybean; GmPDH1 and GmPDH2) and *Medicago truncatula* (Medicago; MtPDH1) preferred prephenate over arogenate as their substrates (Schenck et al., 2015; Schenck et al., 2017a) and, unlike plant ADH enzymes, were insensitive to Tyr inhibition and localized to the cytosol (Schenck et al., 2015; Schenck et al., 2017a). These recently diverged plant ADH and PDH enzymes were used to identify a single

amino acid residue (Asn222 of GmPDH1) of TyrA dehydrogenases that switches TyrA substrate specificity and underlies the evolution of legume PDH enzymes (Schenck et al., 2017a; Schenck et al., 2017b). While these biochemical and evolutionary studies established that some legumes have an alternative Tyr-insensitive cytosolic PDH enzyme, its *in vivo* function is unknown.

To address this issue, we hypothesized and tested four non-mutually exclusive *in planta* functions of the PDH enzyme in legumes. **Hypothesis I: PDH functions as a part of a redundant Tyr biosynthetic pathway in the cytosol** (**Fig. 1**). Although AAA biosynthesis is localized to the plastids (Bickel et al., 1978; Jung et al., 1986), some plants including legumes identified cytosolic isoforms of CM and Tyr-AT, which catalyze immediately up- and down-stream steps of PDH and complete the cytosolic Tyr biosynthetic pathway from chorismate (**Fig. 1**) (D'Amato et al., 1984; Eberhard et al., 1996; Ding et al., 2007; Schenck et al., 2015; Wang et al., 2016). Also, a cytosolic Phe pathway was recently identified in plants (Yoo et al., 2013; Qian et al., 2019). **Hypothesis II: PDH is involved in the production of Tyr or HPP-derived metabolite(s) (Fig. 1).** Tyr is the precursor of many plant specialized metabolites (Schenck and Maeda, 2018) and duplicated primary metabolic enzymes can be co-opted to efficiently provide Tyr and HPP precursors to support their downstream specialized metabolism (Weng et al., 2012; Moghe and Last, 2015; Maeda, 2019). **Hypothesis III: PDH is involved in the Tyr catabolism pathway to the tricarboxylic acid (TCA) cycle.** Tyr catabolism proceeds through HPP, the product of PDH, and feeds intermediates (e.g. fumarate) of the TCA cycle (**Fig. 1**). Thus, HPP produced from PDH may be directly incorporated into the Tyr degradation pathway. **Hypothesis IV: PDH is involved in the legume-rhizobia symbiosis.** Many legumes form a symbiotic relationship with rhizobia, and PDH activity is uniquely present in legumes. Furthermore, *MtPDH1* expression is upregulated in the nodules after treatment with nitrate (NO_3^-, Benedito et al., 2008) or phosphinothricin (PPT, Seabra et al., 2012), both of which

stimulate nodule senescence (Streeter and Wong, 1988; Matamoros et al., 1999; Pérez Guerra et al., 2010). To systematically test the above four hypotheses, this study isolated and characterized *pdh* mutants in the model plant *M. truncatula*, which conveniently has a single *PDH* gene compared with some other legumes that have multiple copies (Schenck et al., 2015; Schenck et al., 2017a) using genetics, biochemistry, metabolomics, histochemical staining, microscopy, and gene expression analyses.

RESULTS

Isolation of pdh mutants in Medicago truncatula

To investigate the *in vivo* function of PDH in legumes, two independent homozygous alleles of *Tnt1*-transposon mutants of *M. truncatula* (Tadege et al., 2008) were identified for the *MtPDH1* locus (Mt3g071980) (Cheng et al., 2014). The *pdh1-1* and *pdh1-2* mutants carried a transposon insertion in the first and last exons of the *MtPDH1* gene, respectively (**Fig. 2a**). *MtPDH1* was constitutively expressed across many tissues and under various conditions with the highest and lowest expression being detected in aerial tissues and seeds, respectively (**Supplementary Fig. 1**). Both alleles did not produce any *PDH* transcript in the leaves (**Fig. 2b**). The *M. truncatula* genome contains two *ADH* genes, *MtADH* (Mt4g115980) and *MtncADH* (Mt5g083530) (Schenck et al., 2017a), but neither were enhanced in the *pdh1* mutants (**Fig. 2b**). Consistent with their transcript levels, PDH activity was almost completely abolished in both *pdh1* mutants without significant reduction in ADH activity (**Fig. 2c**). After six weeks of growth, *pdh1-1* showed no phenotypic difference from wild-type (Wt; R108). The *pdh1-2* mutant, on the other hand, had a slight bushy phenotype, which could be due to an unknown secondary transposon insertion(s) (**Fig. 2d**); however, multiple attempts of backcrossing were unsuccessful. These data provide genetic evidence that *MtPDH* is responsible for the PDH activity detected in *M. truncatula*. The minor impacts of eliminating PDH activity on overall plant growth in two independent *pdh1* mutants suggests that the PDH enzyme is not essential during standard growth conditions in *M. truncatula*.

Tyr and Tyr-derived compounds are unaltered in pdh mutants during standard growth condition

To test the hypothesis that the PDH pathway serves as a redundant Tyr biosynthetic route

(**hypothesis I**), Tyr and Tyr/HPP-derived compounds were analyzed in Wt and mutants. Metabolites were extracted from root and leaf tissue of 6-week-old plants grown under standard conditions. Surprisingly, the levels of Tyr were not significantly different between Wt and mutants in either leaf or root tissue (**Fig. 3a**). Additionally, the levels of Phe and Trp in the leaves and roots were not significantly reduced in mutants as compared to Wt, though a slightly higher Trp level was observed in *pdh1-2* (**Fig. 3a**). Potential effects on tocopherols, HPP-derived metabolites, were also tested (**hypothesis II**), but their levels were not significantly different between Wt and mutants in both leaf and root tissue (**Fig. 3b**). We also performed non-targeted analysis using GC-MS for both polar and non-polar metabolites; however, no consistent differences were observed between Wt and mutants (**Supplementary Table 1**). Together, these data suggest that under standard growth conditions, the lack of the PDH enzyme had no substantial effects on the overall accumulation of aromatic amino acids (AAAs) or Tyr/HPP-derived metabolites analyzed.

In grasses, upwards of 50% of the total lignin is derived from Tyr, via a Tyr ammonia-lyase (TAL) enzyme (Barros et al., 2016). Since TAL activity has also been detected in some non-grass species, including legumes (Giebel, 1973; Beaudoin-Eagan and Thorpe, 1985; Khan et al., 2003), the legume PDH enzyme may synthesize Tyr that is directly incorporated into the phenylpropanoid pathway for downstream products such as lignin (**hypothesis II**). To test this possibility, stem cross-sections from Wt and mutants were stained using two different techniques, Mäule and phloroglucinol, which can detect potential differences in composition or linkages of lignin (Mitra and Loqué, 2014, Pomar et al., 2002). Neither staining method showed any obvious differences in stem lignification between Wt and mutants (**Supplementary Fig. 2a,b**). When phenylpropanoid intermediates, *p*-coumarate and ferulate, involved in lignin biosynthesis were analyzed by GCMS, they were somewhat reduced in *pdh1-2* but not

consistently in *pdh1-1* (**Supplementary Fig. 2c**). Thus, the lack of PDH does not have substantial impacts on lignin biosynthesis in *M. truncatula*.

Less tocopherols are accumulated in pdh1 than Wt under high light treatment.

Under various biotic and abiotic stresses, the shikimate pathway is induced, which often leads to accumulation of AAAs (Dyer et al., 1989; Gilbert et al., 1998; Zhao et al., 1998; Betz et al., 2009). To test the potential role of PDH in Tyr biosynthesis under stress (**hypothesis I**), Wt and *pdh1-1* were subjected to 48-hour high light treatment (Gonzali et al., 2009), which is known to induce production of AAA-derived antioxidants (Collakova and DellaPenna, 2003). The levels of Tyr were not altered, except at 24 hours when Tyr increased slightly in *pdh1-1* compared with Wt (**Supplementary Fig. 3a**). As expected, high light treatment enhanced tocopherol accumulation, but to a significantly lesser extent in *pdh1-1* compared with Wt at both 24 and 48 hours (**Supplementary Fig. 3b**). The levels of anthocyanins, which are also induced under various stresses including high light stress (Collakova and DellaPenna, 2003), were increased after 24 and 48 hours of high light treatment but was not significantly different between Wt and *pdh1-1* (**Supplementary Fig. 3c**). These results show that the lack of PDH negatively impacts the accumulation of HPP-derived tocopherols when their production is induced under high light conditions.

MtPDH1 is co-expressed with senescence-related genes but pdh1 deficiency has no major impacts on dark-induced senescence.

To identify potential processes and pathways that are coordinately regulated with *PDH*, a gene co-expression analysis with *MtPDH1* was performed using the Medicago gene expression atlas (He et al., 2009). *MtPDH1* was co-expressed with genes mainly involved in senescence-related

processes (e.g., nucleases, proteases, and lipases **Supplementary Fig. 1**) and the gene encoding HPP dioxygenase (HPPD, (Siehl et al., 2014), a senescence-activated enzyme involved in Tyr catabolism (**Supplementary Fig. 5a**)(Wang et al., 2019). To experimentally test the potential involvement of PDH in senescence, *PDH* gene expression and enzymatic activity were monitored at different developmental stages during natural leaf senescence (**Supplementary Fig. 4a**). Expression of a senescence marker gene (*MtVPE*, Pérez Guerra et al., 2010) was monitored, together with loss of chlorophyll in leaves collected at various developmental times from a single plant, to define stages of leaf senescence (**Supplementary Fig. 4b**). *MtVPE* was basally expressed in fully green leaves (defined here as the S1 stage), and gradually induced upon senescence (defined here as S2, S3, and S4; **Supplementary Fig. 4b**), mirroring the loss of chlorophyll. Fully senescent leaves (S5) were collected but did not yield high-quality RNA and proteins and were unable to be further analyzed. The highest *MtPDH1* expression was detected in green (S1) leaves, and PDH enzymatic activity was not induced upon senescence (**Supplementary Fig. 4c,d**). Thus, *MtPDH1* is not upregulated during natural senescence in the leaves. Similar to *PDH*, expression of the two *ADH* genes in *M. truncatula* did not follow the developmental pattern of leaf senescence (**Supplementary Fig. 4c**). Unlike PDH activity, however, ADH enzymatic activity was gradually induced upon senescence (**Supplementary Fig. 4d**).

Since *MtPDH1* was co-expressed with *MtHPPD* (**Supplementary Fig. 1**), and PDH together with HPPD provides a direct route for catabolism of Tyr to homogentisate, eventually leading to fumarate (**Fig. 1, Supplementary Fig. 5a**), we investigated potential impacts of *pdh1* deficiency in Tyr catabolism (**hypothesis III**). The expression of genes encoding all enzymes of the Tyr catabolic pathway were measured in the mutants and Wt under standard growth conditions (**Supplementary Fig. 5a**, Dixon and Edwards, 2006). The expression of genes

encoding the first two steps of the pathway, *HPPD* and homogentisate dioxygenase (*HGO*), were not significantly altered in the mutants compared with Wt. The subsequent step, maleylacetoacetate isomerase (*MAAI*), was induced by 2- and 2.5-fold in *pdh1-1* and *pdh1-2*, respectively (**Supplementary Fig. 5b**), though the final step in the pathway, fumarylacetoacetate hydrolase (*FAH*), showed opposite expression patterns in the two mutants (**Supplementary Fig. 5b**). Thus, no consistent changes in the expression of the Tyr degradation pathway genes, beyond *MAAI* were observed in *pdh1* mutants.

To further examine Tyr catabolism during leaf senescence under artificial, but controlled, conditions excised leaves from Wt and mutants were exposed to an extended dark treatment (Xing and Last, 2017; Wang et al., 2019). Over 7 days, leaves from Wt and mutants responded to dark-induced senescence similarly with no apparent growth phenotypes (**Supplementary Fig. 6a**). Furthermore, there were no significant differences in α-tocopherol levels between Wt and mutants at any time point analyzed (**Supplementary Fig. 6b**). These data together suggest that the lack of PDH had no substantial effects on Tyr catabolism or metabolism under standard growth conditions and at least under the senescence conditions tested here (**Supplementary Figs. 5 & 6**).

Less Tyr is accumulated in pdh mutants following shikimate feeding.

Although the steady-state levels of Tyr were not altered in the mutants (**Fig. 3a**), some of the above data suggest that the PDH enzyme may contribute to Tyr production (**hypothesis I**) at least under some stress conditions (**Supplementary Figs. 1 and 3b**). Thus, we hypothesized that the potential role of PDH in Tyr biosynthesis might be manifested when the carbon flux through the Tyr pathway is elevated. To test this possibility, an intermediate of the shikimate pathway, shikimate, was exogenously fed to Wt and mutants and the levels of AAAs were analysed.

Excised leaves were floated in a solution containing shikimate or H_2O for up to 8 hours, rinsed to remove metabolites in the feeding solution, and leaf metabolites were extracted and analyzed using HPLC and GC-MS. As more prolonged feeding with shikimate led to abnormal leaf phenotypes, 8 hours was selected as an optimal time for increased carbon flux without pleiotropic effects. After 8 hours of feeding, shikimate and Phe levels were increased drastically in all genotypes, suggesting that shikimate was taken up and metabolized by the leaves (**Fig. 4**). Tocopherol levels were generally unaffected upon shikimate feeding, likely because the feeding time was not long enough to convert shikimate into tocopherols (**Fig. 4**). Trp levels were reduced in the mutants compared with Wt after feeding with water, and were induced upon shikimate feeding in one mutant (**Fig. 4**). The unexpected differences observed with Trp levels under standard growth conditions (**Fig. 3**) and the feeding experiments (**Fig. 4**) may reflect unknown stress responses during the feeding experiments. Nevertheless, after 8 hours of feeding, Tyr levels increased by >39-fold in Wt, but only by 16- and 13-fold in *pdh1-1* and *pdh1-2*, respectively (**Fig. 4**). Repeated 8 hour shikimate feeding experiments with *pdh1* mutants and Wt yielded similar Tyr accumulation patterns. The difference in the Tyr accumulation suggests that PDH contributes to Tyr biosynthesis when carbon flow through the shikimate pathway is enhanced.

To determine if global metabolite changes occurred after shikimate feeding, additional amino acids and TCA pathway metabolites were analyzed by GC-MS. Interestingly, glutamine levels were higher in H_2O-fed Wt, compared with mutants (**Supplementary Fig. 7**), and upon shikimate feeding, glutamine levels were significantly higher in Wt (**Supplementary Fig. 7**). The levels of TCA cycle intermediates may indicate the functionality of the Tyr catabolic pathway; however, those TCA cycle intermediates analyzed here, including fumararte, were not consistently altered after shikimate feeding in Wt and mutants (**Supplementary Fig. 8**). Citrate levels were reduced in *pdh1-1* and *pdh1-2* compared with Wt in H_2O control treatment; however

after shikimate feeding these differences were no longer apparent (**Supplementary Fig. 8**). These data did not provide evidence to support the involvement of the PDH enzyme in Tyr catabolism to the TCA cycle intermediate.

PDH has limited role in the legume-rhizobia symbiosis

To test if PDH plays a role in legume-rhizobia symbiosis (**hypothesis IV**), Wt plants and *pdh1-1* mutants were grown side-by-side on low nitrogen Fahräeus medium and inoculated with a well-chracterized rhizobium of *M. truncatula*, *Sinorhizobium meliloti* Rm1021. Nodules were counted 14, 21, and 28 days post-inoculation (dpi) and acetylene reduction assays (ARA) were performed to measure nitrogenase activity (Wych and Rains, 1978). At all timepoints *pdh1-1* mutants did not display any phenotypic difference from Wt plants, including the number of nodules produced per root (**Fig. 5a**), suggesting that PDH is not essential for nodule development. *M. truncatula* forms indeterminate nodules that displayed the four standard zones: I, meristematic; II, infection; III, fixation; and IV, senescence zones in both Wt and *pdh1-1* (**Fig. 5b,** Van de Velde et al., 2006). Expression of the bacterial *nifH* gene, which is required for nitrogen fixation, was monitored through the use of a *S. meliloti* strain expressing a P*nifH::uidA* fusion to evaluate nodule maturation on *pdh1-1* and Wt plants (Starker et al., 2006). After 21 and 28 dpi, β-glucuronidase (GUS) activity and the overall nodule development were not altered between *pdh1-1* and Wt (**Fig. 5c**). Although nitrogenase activity in *pdh1-1* appeared to be slightly reduced compared with Wt at 21 and 28 dpi when nodule senescence might have been initiated, no significant differences was observed (**Fig. 5d**). ARA were repeated at the 21 dpi timepoint with *pdh1-1* and this time including *pdh1-2*. Nitrogenase activity was not significantly different between genotypes, even though *pdh1-1* showed a slight reduction, similar to the first experiment (**Fig. 5e**).

Independently, we also measured the presence and absence of PDH from plant tissue extracts of over twenty legume species, which were sampled across the legume phylogeny (Azani et al., 2017, **Supplementary Fig. 9**) and compared with their capacity to form nodules (Afkhami et al., 2018). All legumes sister to previously analyzed *G. max* (soybean) and *M. truncatula* (Schenck et al., 2015) showed PDH activity including *Arachis ipaensis* (peanut), which possess a TyrA enzyme with similar ADH and PDH activity (Schenck et al, 2017). All of these legumes were previously reported to be able to nodulate (Afkhami et al., 2018). When four legume species in the genistoid crown were analyzed (e.g. *Lupinus polyphyllus*), PDH activity was not detectable in any of them, despite successful detection ADH activity (**Supplementary Fig. 9**). Importantly, these legumes were reported to be able to nodulate, suggesting that legume plants having undetectable levels of PDH activity can still maintain nodulation. Some early diverging legume lineages are known to nodulate. Out of four of these species sampled from the mimosid crown three showed PDH activity (**Supplementary Fig. 9**). In contrast, all four species from caesalpinioid, another early diverging legume clade, are incapable of nodulating (Afkhami et al., 2018), but showed PDH activity (**Supplementary Fig. 9**). The lack of detectable PDH activity (e.g. in the genistoid crown) may be simply due to insuffient sensitivity with HPLC-based assay and/or the use of tissues that do not necessarily express *PDH*. However, detection of PDH activity in species lacking nodulation (e.g. in the caesalpinioid node) strongly support the lack of positive correlation between the presence of PDH activity and nodulation across the legume phylogeny. Phylogenetic sampling (**Supplementary Fig. 9**) together with *pdh1* mutant analysis (**Fig. 5**) together suggest that PDH is not essential for legume-rhizobia symbiosis, though more detailed analyses are needed to fully address its contribution to potentially enhance nitrogen fixation within the nodules in some legumes.

319

320

321

322

DISCUSSION:

In this study, we sought to understand the function of legume-specific PDH enzymes through analysis of *Tnt1*-transposon mutants of *PDH* in *M. truncatula*. Not only is *M. truncatula* a convenient model system having mutant populations and many genomic/transcriptomic resources, but *M. truncatula* also has a single *PDH* gene unlike some other legumes, i.e., soybean, having two *PDH* genes (Schenck et al., 2015). Analysis of two independent *pdh1* mutant lines suggests that MtPDH1 is responsible for all the PDH activity in *M. truncatula* (**Fig. 1**). This observation is consistent with chromatographic separation of PDH from ADH in soybean, which resulted in the detection of a single PDH peak as compared to multiple ADH peaks (Schenck et al., 2015). Our genetic data also support that ncADH, and ADH enzymes do not contribute to PDH activity, in agreement with *in vitro* data of soybean and *M. truncatula* enzymes (Schenck et al., 2015; Schenck et al., 2017a).

Surprisingly, the null *pdh1* mutants, displayed no visible aberrant growth phenotypes (**Fig. 1**). A slight bushy phenotype was observed in the *pdh1-2* allele, but not in *pdh1-1*, and thus here we focused on consistent responses observed in both alleles to avoid potential pleiotropic effects specific to *pdh1-2*. The lack of substantial phenotypes in *pdh1* is in contrast to the highly compromised growth and leaf development phenotypes of Arabidopsis *adh2/tyra2* mutant (de Oliveira et al., 2019). In *M. truncatula*, we were also unable to recover homozygous mutants of the canonical *ADH*, which is a single copy gene in *M. truncatula* as compared to two *ADH* copies present in Arabidopsis (Rippert and Matringe, 2002), further suggesting the essential nature of the ADH-mediated Tyr pathway in legumes. Thus, the canonical plastid-localized ADH pathway is the predominant Tyr biosynthetic route and cannot be compensated by the cytosolic PDH pathway in legumes.

Using the *pdh1* mutants, this study further systematically evaluated potential roles of

PDH in Tyr biosynthesis (**hypothesis I**), biosynthesis of Tyr- and HPP-derived metabolites (**II**), Tyr catabolism and senescence (**III**), and legume-rhizobia symbiosis (**IV**). The obtained data provide evidence for support of **hypothesis I** that the PDH enzyme is involved in Tyr biosynthesis when carbon flux is increased through the shikimate pathway. Although Tyr levels were not altered between Wt and mutants under standard conditions (**Fig. 3a**), upon feeding with shikimate, Wt accumulated over 2-fold more Tyr than *pdh1-1* and *pdh1-2* (**Fig. 4**). Although AAA biosynthesis is localized to the plastids (Bickel et al., 1978; Jung et al., 1986; Maeda and Dudareva, 2012), some isoforms of the shikimate and AAA pathway enzymes were detected in the cytosol (Rubin and Jensen, 1985; Ganson et al., 1986; Ding et al., 2007). Cytosolic CM activities have been detected from various plant species including soybean (Goers and Jensen, 1984; Kuroki and Conn, 1989; Mobley et al., 1999; Schenck et al., 2015), which are not regulated by the AAAs, unlike their plastidic counterparts (Eberhard et al., 1996; Mobley et al., 1999; Westfall et al., 2014). Tyr-insensitive PDH enzymes provide a cytosolic route for conversion of prephenate into HPP, which can be further transaminated to Tyr by cytosolic Tyr-AT enzymes (**Fig. 1**) (Wang et al., 2016). Although the PDH-mediated Tyr pathway is not the predominant route for Tyr biosynthesis, it may provide an alternative route for additional Tyr synthesis under some conditions that increase flux through the shikimate pathway.

The current data also partly support **hypothesis II** that the PDH enzyme contributes to the production of specialized metabolites derived from Tyr and/or HPP in legumes. Although Tyr/HPP-derived tocopherols were not altered in the *pdh1* mutants under standard growth conditions (Fig. 3b), high light-induced tocopherol accumulation was partially attenuated in the *pdh1* mutant (**Supplementary Figure 3**). Therefore, the PDH enzyme may also contribute to tocopherol biosynthesis under stress conditions. Some specialized metabolic pathways emerged through duplication and neofunctionalization of genes from primary metabolic pathways (Weng

et al., 2012; Moghe and Last, 2015). The legume PDH enzyme emerged as the result of a recent gene duplication of an *ADH* gene followed by a shift in substrate specificity from arogenate to prephenate (Schenck et al., 2017a). Thus, legumes may be able to divert the shikimate pathway flux to provide additional HPP or Tyr in the cytosol for the synthesis of downstream specialized metabolites including tocopherols. To further test this possibiliy, additional metabolomics experiments were conducted, but did not identify any putative HPP-derived compounds that were absent or lower in *pdh1* mutants than Wt (**Supplementary Table 1**). Although there are many Tyr and HPP-derived specialized metabolites produced in plants (e.g., rosmarinic acid, betalains, dhurrin, and benzylisoquinoline alkaloids), none appear to be specific to the legume lineage or correlate with the distribution of PDH activity (**Supplementary Fig. 9**) (Schenck and Maeda, 2018). Some species of the legume genus *Inga* can accumulate Tyr to 20% of leaf dry weight, which deters insect predation (Lokvam et al., 2006). Further analysis identified *Inga* species with high *PDH* expression that have hyper-accumulation of Tyr-derived specialized metabolites, such as Tyr-gallates (Coley et al., 2019). Therefore, more comprehensive analyses of Tyr-derived metabolites under different conditions, tissues types, and other legume species may identify specialized metabolites derived from the PDH enzyme in legumes.

The current data did not provide sufficient support for **hypothesis III** that the PDH pathway potentially contributes to Tyr catabolism and senescence. As Tyr is the most energetic amino acid (Hildebrandt et al., 2015), its catabolism is a crucial process in recovering energy. Mutations in Tyr catabolic genes can have dramatic effects of plant development (Han et al., 2013). Tyr is catabolized into fumarate, a TCA pathway intermediate, first by conversion into HPP via a Tyr-AT enzyme and further through the canonical Tyr catabolism pathway (**Supplementary Fig. 5a**) (Hildebrandt et al., 2015). Knockout of a soybean *HGO* did not cause lethality but led to an increase in vitamin E content by 2-fold, suggesting that a significant

amount of carbon flux is diverted into vitamin E production when Tyr catabolism is blocked (Stacey et al., 2016). Furthermore, *MtPDH1* was co-expressed with *HPPD*, which together provide a direct pathway for homogentisate production. This potential coordination of PDH and HPPD, and cytosolic localization, can bypass three enzymatic steps of the ADH-mediated Tyr biosynthetic pathway, catalyzed by PPA-AT, ADH, and Tyr-AT to enter into the canonical Tyr catabolism pathway (**Fig. 1 & Supplementary Fig. 5a**). Additionally, *PDH* was co-expressed with many senescence-related genes (**Supplementary Fig. 1**, Van de Velde et al., 2006; Kusaba et al., 2013; Xi et al., 2013) suggesting that *PDH* may function when Tyr catabolism is enhanced. Despite these correlative data, however, experiments designed here to test the potential link between PDH and senescence did not provide evidence to support this hypothesis: upon dark-induced (**Supplementary Fig. 6**) and natural senescence (**Supplementary Fig. 4**) conditions that likely stimulate Tyr catabolism, no phenotypic differences were observed between mutants and Wt. Also, genes involved in Tyr catabolism were not consistently altered in mutants as compared to Wt (**Supplementary Fig. 5b**), and PDH expression and enzymatic activity were not induced upon senescence (**Supplementary Fig. 4c**). Thus, further experiments under different conditions (e.g. specific stress that induces Tyr catabolism) are needed to address the potential role of PDH in Tyr catabolism and senescence.

The data obtained in this study failed to directly support the **hypothesis IV** that the PDH pathway plays a role in legume-rhizobia symbiosis. Legumes initiate a symbiotic relationship with soil-dwelling rhizobia when there is insufficient nitrogen (Oldroyd et al., 2011). A chemical communication ensues that ultimately results in compatible rhizobia invading legume roots and formation of a new organ, the root nodule (Oldroyd, 2013). In the nodule, rhizobia fix atmospheric dinitrogen into ammonium, which is assimilated by the plant through the glutamine synthetase-glutamine oxoglutarate aminotransferase (GS-GOGAT) cycle, in which glutamine and

glutamate are key amino acid carriers (Krapp, 2015). Mutations in *MtPDH1* did not alter nodule numbers (**Fig. 5a**) or the developmental progression of the nodules (**Fig. 5c**). Furthermore, nitrogenase activity was not significantly affected in mutants at any stage during the symbiotic interaction even when senescence might have been initiated (**Figs. 5d,e**). Alterations in nitrogen assimilation can lead to reduced nodulation in legumes (Streeter and Wong, 1988; Matamoros et al., 1999): for example, plants treated with a GS inhibitor phosphinothricin (PPT) result in loss of nodulation (Seabra et al., 2012) and also stimulate *MtPDH1* expression (**Supplementary Fig. 1**) as well as many other genes. Interestingly, *pdh1-1* and *pdh1-2* had reduced glutamine levels in the H_2O-treated control leaves after 8 hours (**Supplementary Fig. 7**), which also persisted after shikimate feeding (**Supplementary Fig. 7**). Reduced glutamine levels in the *pdh1* mutants may, in turn, affect the symbiotic efficiency with rhizobia, although no statistically-significant reduction in nitrogenase activity was observed (**Figs. 5d,e**). Furthermore, PDH activity, which was measured in a phylogenetically diverse group of legumes, does not correlate with ability to nodulate (Azani et al., 2017; Afkhami et al., 2018, **Supplementary Fig. 9**). Thus, although PDH may provide an adaptive advantage to some legumes, it is likely not directly involved in and essential for the legume-rhizobia symbiosis.

441 **FIGURES:**

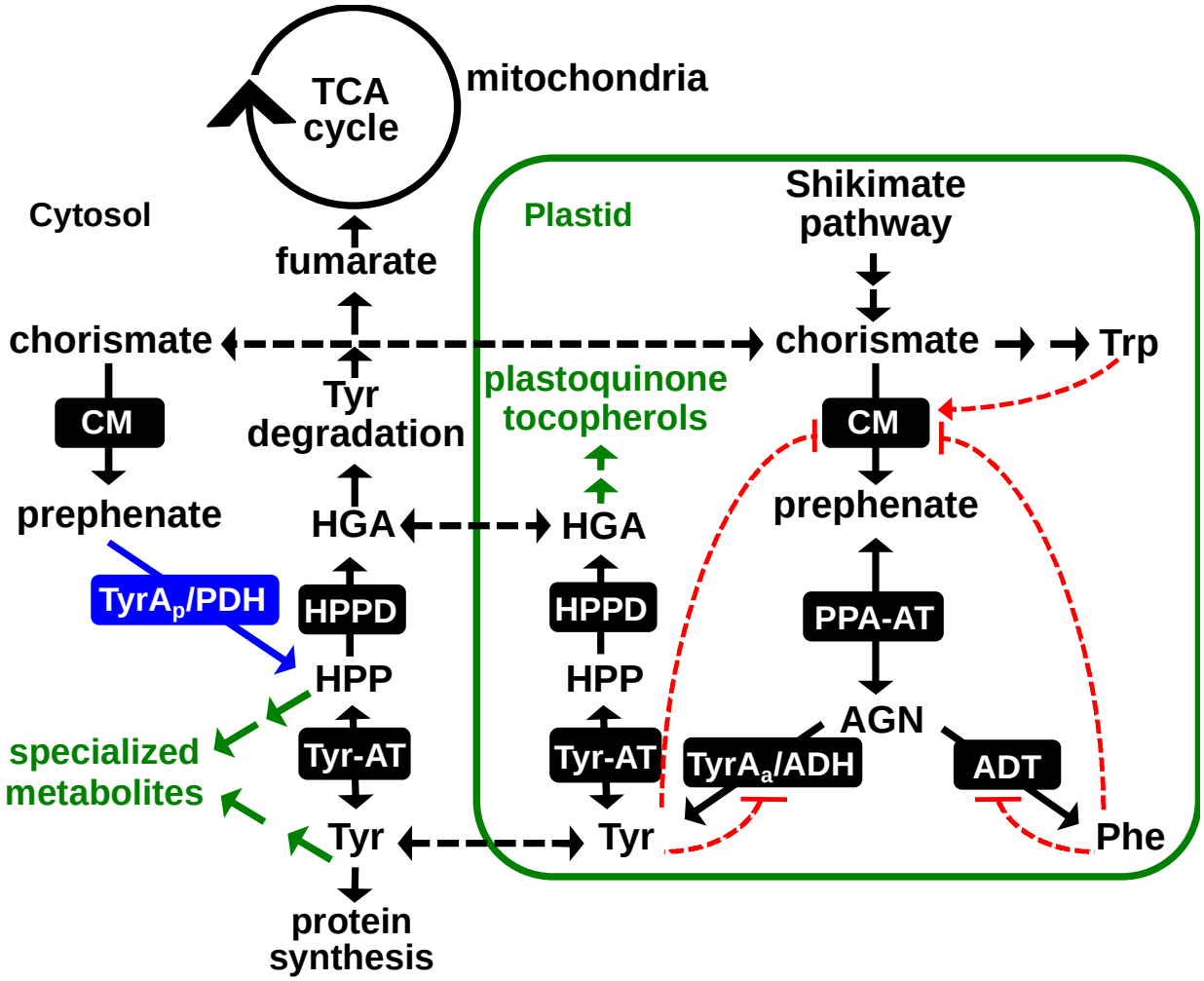

442

443 **Figure 1. Tyr biosynthesis in legumes.** In addition to a highly regulated plastid localized ADH pathway
444 for Tyr biosynthesis, legumes possess a Tyr-insensitive, cytosolic PDH enzyme (blue). Tyr synthesized in
445 the plastids is exported into the cytosol where it can be incorporated into proteins, enter the Tyr degradation
446 pathway to the TCA cycle or serve as a precursor to specialized metabolism. Black dotted lines denote
447 known or potential transport steps, red dotted lines represent feedback regulation with arrows meaning
448 induction and hashes inhibition. AGN, arogenate; ADT, arogenate dehydratase; CM, chorismate mutase;
449 HGA, homogentisate; HPP, 4-hydroxyphenylpyruvate; HPPD, HPP dioxygenase; PPA-AT, prephenate
450 aminotransferase; $TyrA_a$/ADH, arogenate dehydrogenase; $TyrA_p$/PDH, prephenate dehydrogenase;
451 Tyr-AT, tyrosine aminotransferase.

452

453

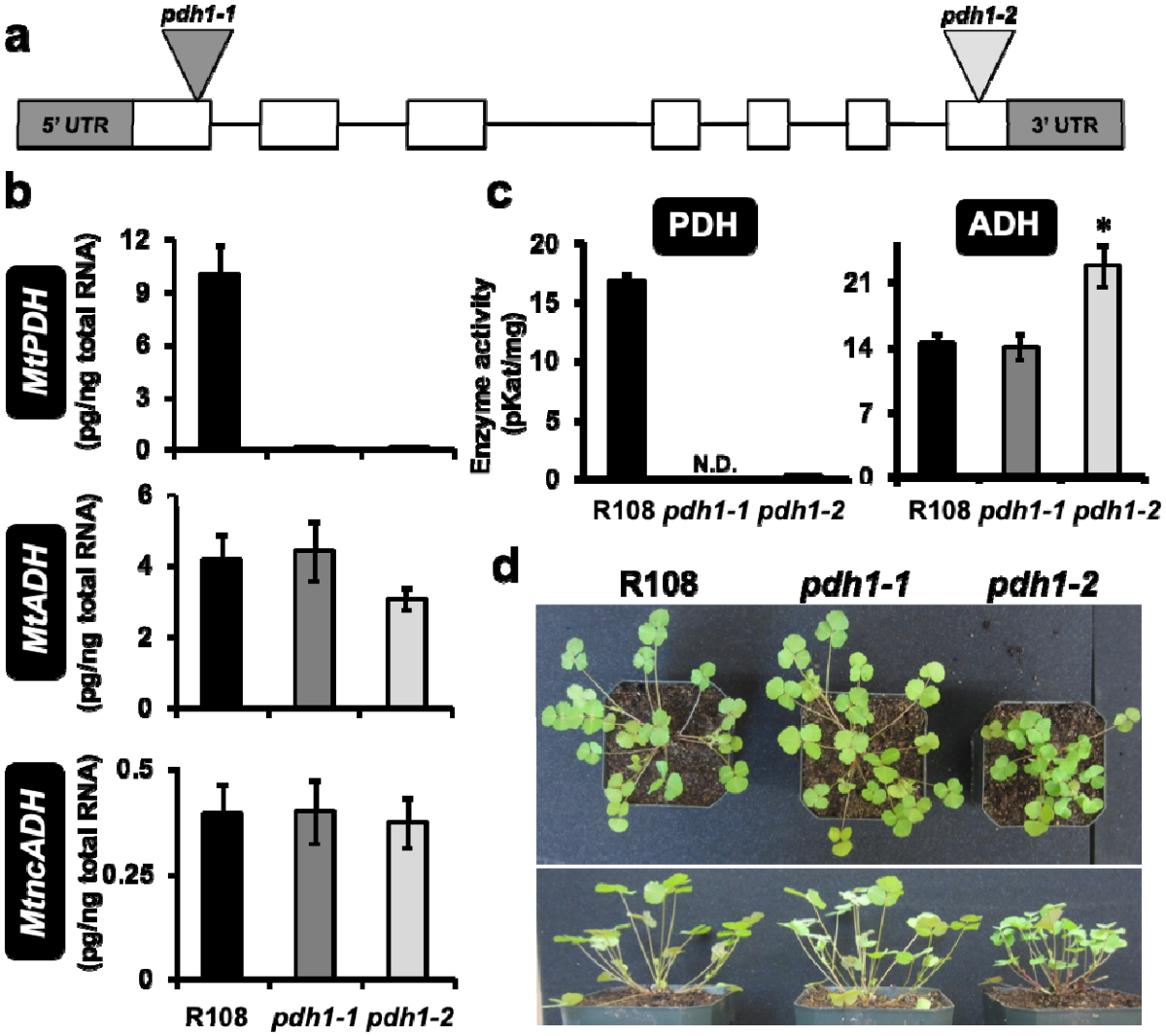

Figure 2. Isolation of *MtPDH1* mutants. (a) *MtPDH1* (Mt3g071980) genomic structure, exons (white boxes) and introns (lines), 5' and 3' untranslated regions (UTR, gray boxes). Two *Tnt1*-transposon mutants were isolated with insertions in exon one (*pdh1-1*) and seven (*pdh1-2*). **(b)** *MtPDH1* transcripts were nearly abolished in *pdh1-1* and *pdh1-2*, without effecting expression of either *ADH* homolog. Bars represent average absolute mRNA levels (pg/ng total RNA) ± s.e.m of n = 3 biological replicates. **(c)** PDH and ADH activity from mutants and wild-type (Wt, R108). Bars represent average enzymatic activity (pKat mg^{-1}) ± s.e.m of n = 3 biological replicates. Significant differences to R108 control are indicated; *$P \leq 0.05$. **(d)** Phenotype of R108 and mutants after 6-weeks growth under standard conditions.

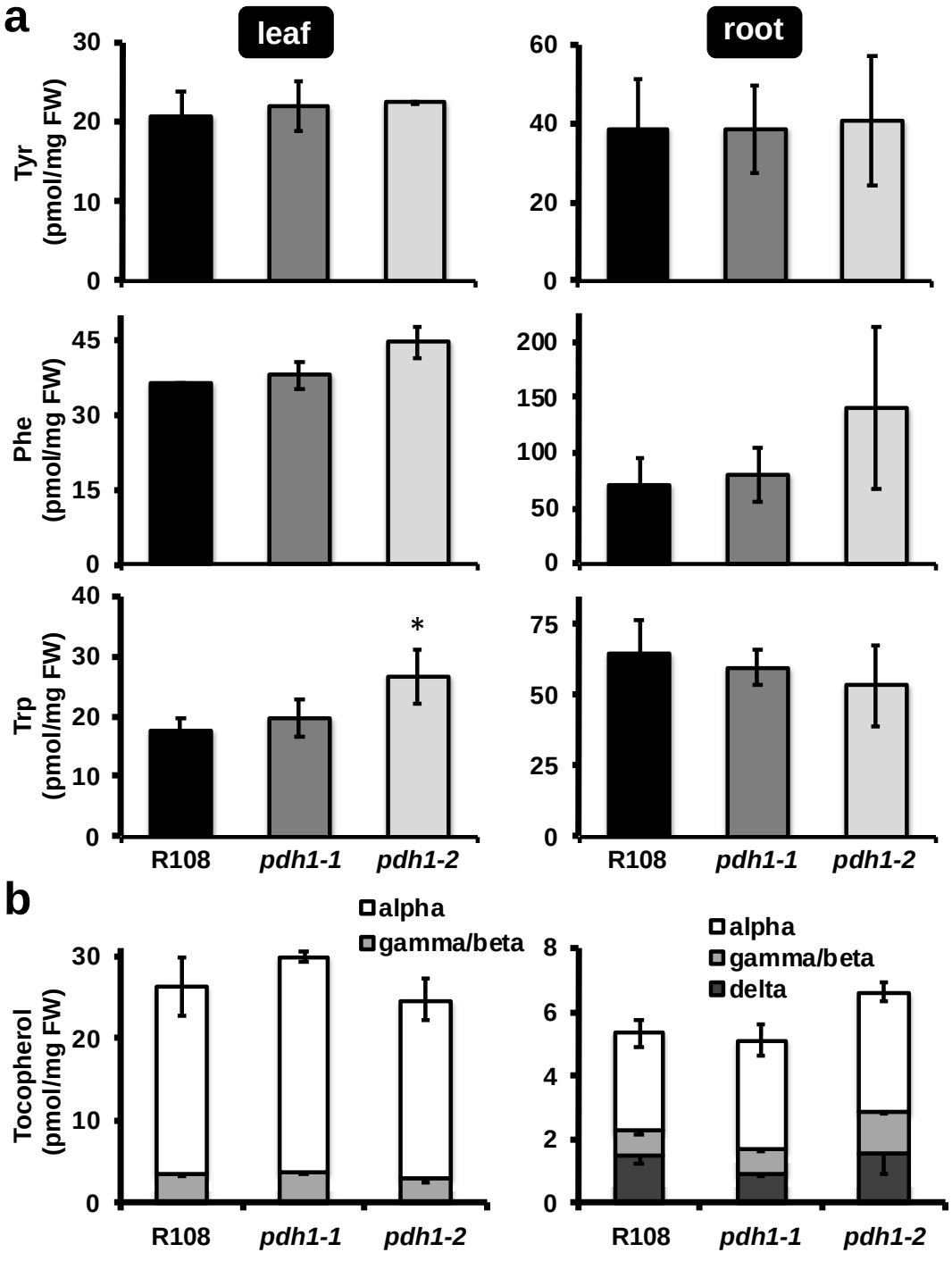

Figure 3. Targeted metabolite analysis of *mtpdh1* mutants and Wt. Leaf and root tissue from 6-week-old plants, grown under standard conditions were used for metabolite extraction. Bars represent average absolute metabolite levels (pmol/mg fresh weight (FW)) ± s.e.m of n = 3 biological replicates. **(a)** Aromatic amino acid levels in leaf and root tissue. Significant differences to Wt (R108) control are indicated; $*P \leq 0.05$. **(b)** Tocopherol composition and content from leaf and root tissue.

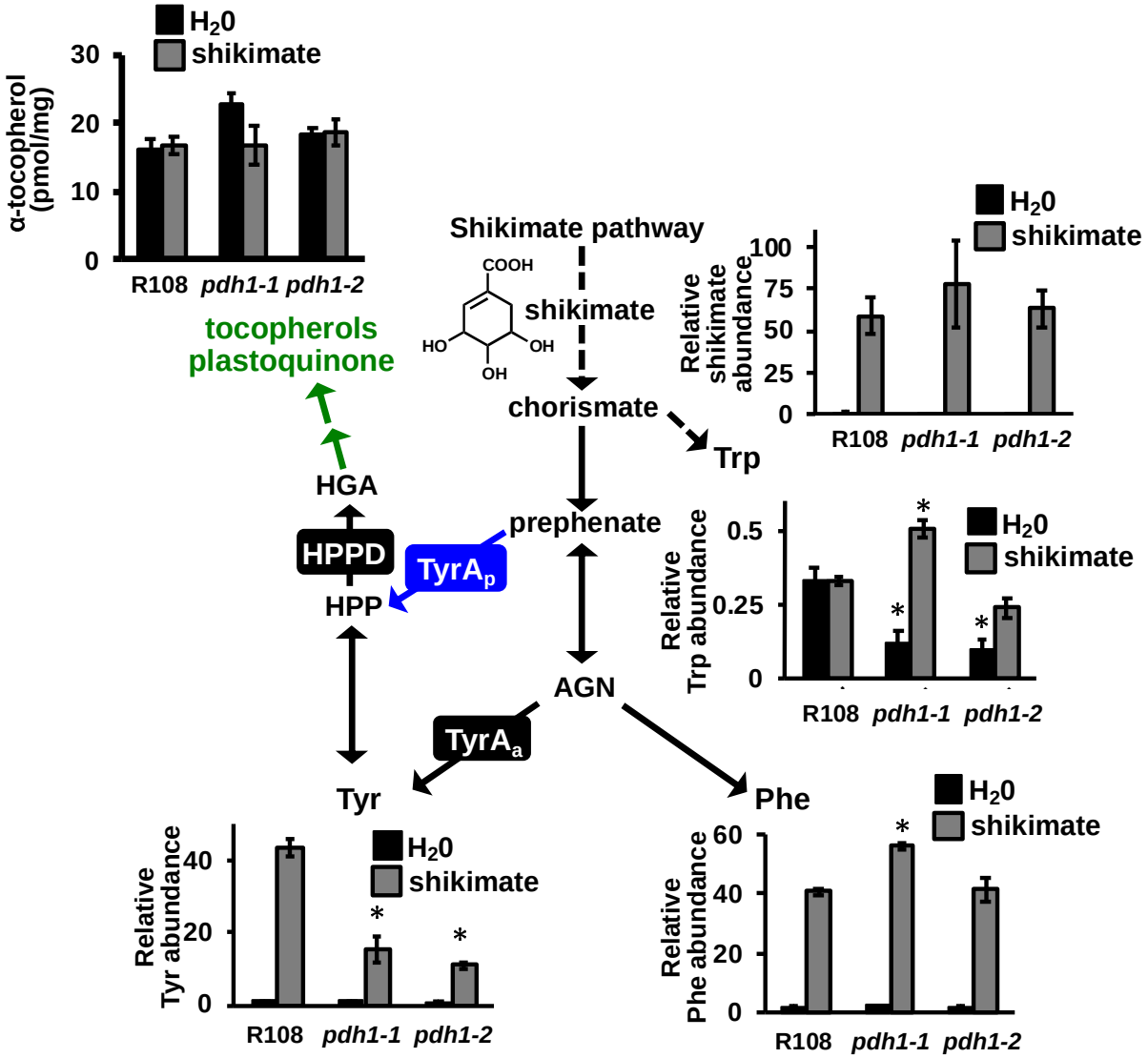

Figure 4. Metabolite analysis after shikimate feeding in Wt and *mtpdh1* mutants. Excised leaves from 6-week-old plants were floated on a solution containing H_20 (black bars) or 25 mM shikimate (gray bars) for 8 hours under constant light. Leaves were then used for metabolite analysis using GC-MS (Tyr, Trp, Phe and shikimate) or HPLC (α-tocopherol). Bars represent average relative metabolite abundance of Tyr, Phe, Trp and shikimate ± s.e.m of n = 3 biological replicates. α-tocopherol is shown as the average absolute metabolite abundance in pmol/mg FW ± s.e.m of n = 3 biological replicates. Additional metabolites after shikimate feeding are shown in **Supplementary Figures 8 & 9**. Significant differences to Wt (R108) control are indicated; *$P \leq 0.05$.

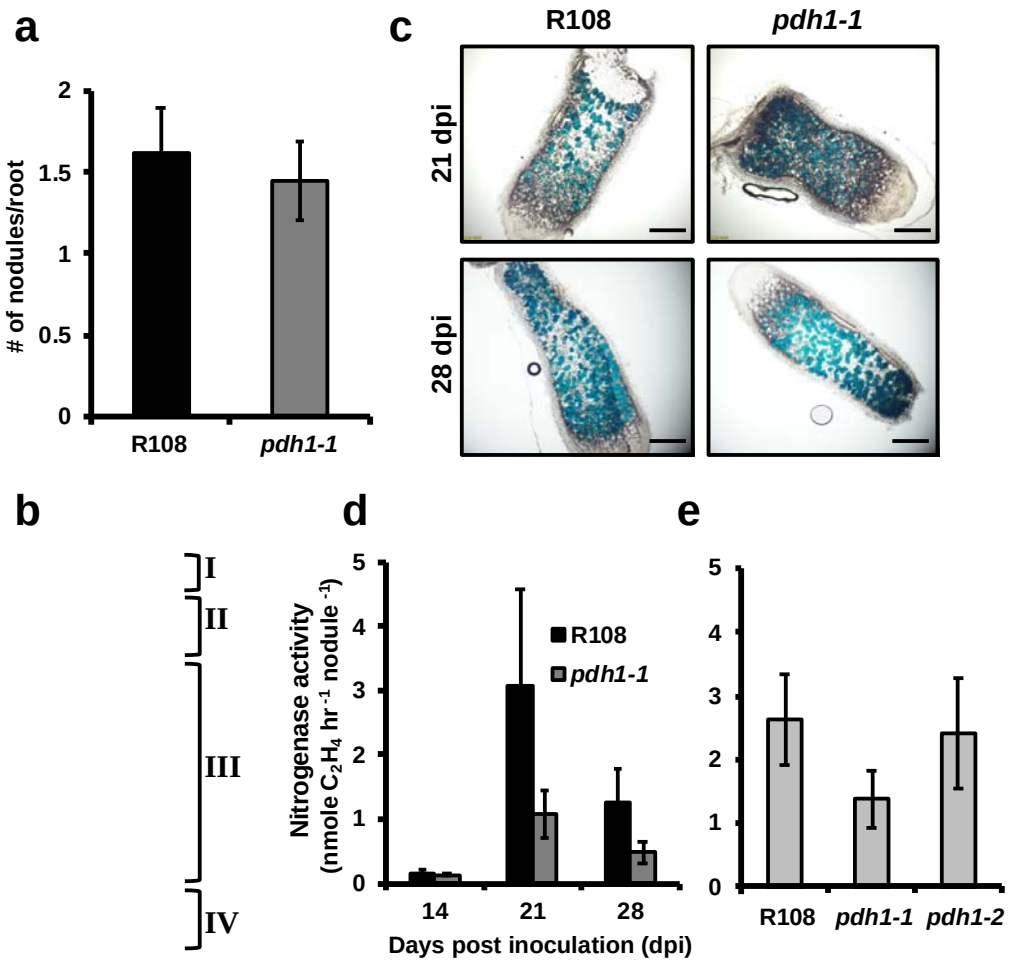

Figure 5. The role of PDH in legume-rhizobia symbiosis. (a) Wt and *pdh1-1* were grown on plates with low nitrogen Fahräeus medium, and 14 days post inoculation (dpi) with *S. meliloti* nodules were counted. Bars represent average number of nodules per root ± s.e.m. with n > 11 plants. **(b)** Indeterminate nodules from *M. truncatula* consist of four developmental zones. I meristem, II infection, III fixation, and IV senescence located closest to the root. These four developmental zones are shown on a characteristic nodule (enlarged for visualization) from 28 dpi. GUS staining with P*nifH*::UidA shows expression of bacterial *nifH* gene localized to the bacteroids (blue). **(c)** Thin sections of nodules from 21 and 28 dpi showing expression of P*nifH*::UidA, highlight bacteroid and nodule development in R108 and *pdh1-1*. Approximately equal staining was observed in all nodule developmental zones, suggesting *pdh1-1* is not affected in nodule development or bacteroid number, scale bar = 1 mM. **(d)** Nitrogen fixation efficiency was measured using an acetylene reduction assay (ARA). Plants were grown under the same conditions as in **a**, 14, 21 and 28 dpi ethylene production was measured and expressed as the average ± s.e.m with n > 7. **(e)** Nitrogen fixation efficiency assay performed in the same way as in **(d)** however, only at 21 dpi and with both mutant alleles and Wt. Activity is expressed as the average ± s.e.m with n > 4.

Acknowledgements:

This work was supported by grants from the National Science Foundation IOS-1354971 to H.A.M. and NSF#1331098 and NSF#1546742 to JMA. LWS is supported in part by NSF awards 1340058, 1743594, 1139489, and 1639618. The University of Missouri, Office of Research provided initial instrumental and personnel funding for the MU Metabolomics Center. Development of *M. truncatula Tnt1* mutant population was, in part, funded by the National Science Foundation, USA (DBI-0703285 and IOS-1127155) to KSM. We thank the Germplasm Resources Information Network (GRIN) for providing some of the legume seeds used in this study.

Conflict of Interest Statement:

The authors declare no conflicts of interest.

Aurthor Contribution:

CAS, JW, DJ, and KG carried our experiments and interpreted results. CAS, JMA, LWS, and HAM designed experiments. KSM and JW developed *Tnt1* mutant lines. CAS and HAM wrote the manuscript. All authors read and edited the manuscript.

REFERENCES:

Afkhami ME, Luke Mahler D, Burns JH, Weber MG, Wojciechowski MF, Sprent J, Strauss SY (2018) Symbioses with nitrogen-fixing bacteria: nodulation and phylogenetic data across legume genera. Ecology **99**: 502

Azani N, Babineau M, Bailey CD, Banks H, Barbosa AR, Pinto RB, Boatwright JS, Borges LM, Brown GK, Bruneau A, et al (2017) A new subfamily classification of the Leguminosae based on a taxonomically comprehensive phylogeny: The Legume Phylogeny Working Group (LPWG). TAXON **66**: 44–77

Barken I, Geller J, Rogosnitzky M (2008) Noscapine inhibits human prostate cancer progression and metastasis in a mouse model. Anticancer Res **28**: 3701–3704

Barros J, Serrani-Yarce JC, Chen F, Baxter D, Venables BJ, Dixon RA (2016) Role of bifunctional ammonia-lyase in grass cell wall biosynthesis. Nat Plants **2**: 16050

Beaudoin GAW, Facchini PJ (2014) Benzylisoquinoline alkaloid biosynthesis in opium poppy. Planta **240**: 19–32

Beaudoin-Eagan LD, Thorpe TA (1985) Tyrosine and phenylalanine ammonia lyase activities during shoot initiation in tobacco callus cultures. Plant Physiol **78**: 438–441

Benedito VA, Torres-Jerez I, Murray JD, Andriankaja A, Allen S, Kakar K, Wandrey M, Verdier J, Zuber H, Ott T, et al (2008) A gene expression atlas of the model legume *Medicago truncatula*. Plant J Cell Mol Biol **55**: 504–513

Betz GA, Gerstner E, Stich S, Winkler B, Welzl G, Kremmer E, Langebartels C, Heller W, Sandermann H, Ernst D (2009) Ozone affects shikimate pathway genes and secondary metabolites in saplings of European beech (*Fagus sylvatica* L.) grown under greenhouse conditions. Trees **23**: 539–553

Bickel H, Palme L, Schultz G (1978) Incorporation of shikimate and other precursors into aromatic amino acids and prenylquinones of isolated spinach chloroplasts. Phytochemistry **17**: 119–124

Bramley PM, Elmadfa I, Kafatos A, Kelly FJ, Manios Y, Roxborough HE, Schuch W, Sheehy PJA, Wagner K-H (2000) Vitamin E. J Sci Food Agric **80**: 913–938

Catoira R, Galera C, de Billy F, Penmetsa RV, Journet EP, Maillet F, Rosenberg C, Cook D, Gough

C, Dénarié J (2000) Four genes of *Medicago truncatula* controlling components of a nod factor transduction pathway. Plant Cell **12**: 1647–1666

Cheng X, Wang M, Lee H-K, Tadege M, Ratet P, Udvardi M, Mysore KS, Wen J (2014) An efficient reverse genetics platform in the model legume *Medicago truncatula*. New Phytol **201**: 1065–1076

Coley PD, Endara M-J, Ghabash G, Kidner CA, Nicholls JA, Pennington RT, Mills AG, Soule AJ, Lemes MR, Stone GN, et al (2019) Macroevolutionary patterns in overexpression of tyrosine: an anti-herbivore defence in a speciose tropical tree genus, *Inga* (Fabaceae). J Ecol **107**: 1620–1632

Collakova E, DellaPenna D (2003) Homogentisate phytyltransferase activity is limiting for tocopherol biosynthesis in Arabidopsis. Plant Physiol **131**: 632–642

Connelly JA, Conn EE (1986) Tyrosine biosynthesis in *Sorghum bicolor*: isolation and regulatory properties of arogenate dehydrogenase. Z Naturforschung C J Biosci **41**: 69–78

D'Amato T, Ganson RJ, Gaines C, Jensen R (1984) Subcellular localization of chorismate-mutase isoenzymes in protoplasts from mesophyll and suspension-cultured cells of *Nicotiana silvestris*. Planta **162**: 104–108

Ding L, Hofius D, Hajirezaei M-R, Fernie AR, Börnke F, Sonnewald U (2007) Functional analysis of the essential bifunctional tobacco enzyme 3-dehydroquinate dehydratase/shikimate dehydrogenase in transgenic tobacco plants. J Exp Bot **58**: 2053–67

Dixon DP, Edwards R (2006) Enzymes of tyrosine catabolism in *Arabidopsis thaliana*. Plant Sci **171**: 360–366

Dyer WE, Henstrand JM, Handa AK, Herrmann KM (1989) Wounding induces the first enzyme of the shikimate pathway in Solanaceae. Proc Natl Acad Sci U S A **86**: 7370–7373

Eberhard J, Ehrler T, Epple P, Felix G, Raesecke H-R, Amrhein N, Schmid J (1996) Cytosolic and plastidic chorismate mutase isozymes from *Arabidopsis thaliana*: molecular characterization and enzymatic properties. Plant J **10**: 815–821

Fitzpatrick PF (1999) Tetrahydropterin-dependent amino acid hydroxylases. Annu Rev Biochem **68**: 355–381

Gaines CG, Byng GS, Whitaker RJ, Jensen RA (1982) L-Tyrosine regulation and biosynthesis via arogenate dehydrogenase in suspension-cultured cells of *Nicotiana silvestris* Speg. et Comes.

572 Planta **156**: 233–240

573 **Gamborg OL, Keeley FW** (1966) Aromatic metabolism in plants I. A study of the prephenate
574 dehydrogenase from bean plants. Biochim Biophys Acta **115**: 65–72

575 **Ganson RJ, D'Amato TA, Jensen RA** (1986) The two-isozyme system of
576 3-deoxy-d-arabino-heptulosonate 7-phosphate synthase in *Nicotiana silvestris* and other higher
577 plants. Plant Physiol **82**: 203–10

578 **Giebel J** (1973) Phenylalanine and tyrosine ammonia-lyase activities in potato roots and their significance
579 in potato resistance to *Heterodera rostochiensis*. Nematologica **19**: 3–6

580 **Gilbert GA, Gadush MV, Wilson C, Madore MA** (1998) Amino acid accumulation in sink and source
581 tissues of *Coleus blumei* Benth. during salinity stress. J Exp Bot **49**: 107–114

582 **Goers SK, Jensen RA** (1984) Separation and characterization of two chorismate-mutase isoenzymes
583 from *Nicotiana silvestris*. Planta **162**: 109–116

584 **Gonzali S, Mazzucato A, Perata P** (2009) Purple as a tomato: towards high anthocyanin tomatoes.
585 Trends Plant Sci **14**: 237–241

586 **Han C, Ren C, Zhi T, Zhou Z, Liu Y, Chen F, Peng W, Xie D** (2013) Disruption of fumarylacetoacetate
587 hydrolase causes spontaneous cell death under short-day conditions in Arabidopsis. Plant Physiol
588 **162**: 1956–1964

589 **Hardy RWF, Holsten RD, Jackson EK, Burns RC** (1968) The acetylene-ethylene assay for N2 fixation:
590 laboratory and field evaluation. Plant Physiol **43**: 1185–1207

591 **He J, Benedito VA, Wang M, Murray JD, Zhao PX, Tang Y, Udvardi MK** (2009) The *Medicago*
592 *truncatula* gene expression atlas web server. BMC Bioinformatics **10**: 441

593 **Higuchi T, Ito Y, Kawamura I** (1967) *p*-hydroxyphenylpropane component of grass lignin and role of
594 tyrosine-ammonia lyase in its formation. Phytochemistry **6**: 875–881

595 **Hildebrandt TM, Nunes Nesi A, Araújo WL, Braun H-P** (2015) Amino acid catabolism in plants. Mol
596 Plant **8**: 1563–79

597 **Jung E, Zamir LO, Jensen RA** (1986) Chloroplasts of higher plants synthesize L-phenylalanine via
598 L-arogenate. Proc Natl Acad Sci U S A **83**: 7231–7235

Khan W, Prithiviraj B, Smith DL (2003) Chitosan and chitin oligomers increase phenylalanine ammonia-lyase and tyrosine ammonia-lyase activities in soybean leaves. J Plant Physiol **160**: 859–863

Krapp A (2015) Plant nitrogen assimilation and its regulation: a complex puzzle with missing pieces. Curr Opin Plant Biol **25**: 115–122

Kries H, O'Connor SE (2016) Biocatalysts from alkaloid producing plants. Curr Opin Chem Biol **31**: 22–30

Kryvoruchko IS, Sinharoy S, Torres-Jerez I, Sosso D, Pislariu CI, Guan D, Murray J, Benedito VA, Frommer WB, Udvardi MK (2016) MtSWEET11, a nodule-specific sucrose transporter of *Medicago truncatula*. Plant Physiol **171**: 554–565

Kuroki GW, Conn EE (1989) Differential activities of chorismate mutase isozymes in tubers and leaves of *Solanum tuberosum* L. Plant Physiol **89**: 472–6

Kusaba M, Tanaka A, Tanaka R (2013) Stay-green plants: what do they tell us about the molecular mechanism of leaf senescence. Photosynth Res **117**: 221–234

Lee J, Durst RW, Wrolstad RE (2005) Determination of total monomeric anthocyanin pigment content of fruit juices, beverages, natural colorants, and wines by the pH differential method: collaborative study. J AOAC Int **88**: 1269–1278

Lokvam J, Brenes-Arguedas T, Lee JS, Coley PD, Kursar TA (2006) Allelochemic function for a primary metabolite: the case of L-tyrosine hyper-production in *Inga umbellifera* (Fabaceae). Am J Bot **93**: 1109–1115

Maeda H, Dudareva N (2012) The shikimate pathway and aromatic amino acid biosynthesis in plants. Annu Rev Plant Biol **63**: 73–105

Maeda H, Yoo H, Dudareva N (2011) Prephenate aminotransferase directs plant phenylalanine biosynthesis via arogenate. Nat Chem Biol **7**: 19–22

Maeda HA (2019) Evolutionary diversification of primary metabolism and Its contribution to plant chemical diversity. Front Plant Sci. doi: 10.3389/fpls.2019.00881

Matamoros MA, Baird LM, Escuredo PR, Dalton DA, Minchin FR, Iturbe-Ormaetxe I, Rubio MC, Moran JF, Gordon AJ, Becana M (1999) Stress-induced legume root nodule senescence.

physiological, biochemical, and structural alterations. Plant Physiol **121**: 97–112

Metz JG, Nixon PJ, Rogner M, Brudvig GW, Diner BA (1989) Directed alteration of the D1 polypeptide of photosystem II: evidence that tyrosine-161 is the redox component, Z, connecting the oxygen-evolving complex to the primary electron donor, P680. Biochemistry **28**: 6960–6969

Mitra PP, Loqué D (2014) Histochemical staining of *Arabidopsis thaliana* secondary cell wall elements. JoVE J Vis Exp e51381–e51381

Mobley EM, Kunkel BN, Keith B (1999) Identification, characterization and comparative analysis of a novel chorismate mutase gene in *Arabidopsis thaliana*. Gene **240**: 115–23

Moghe GD, Last RL (2015) Something old, something new: conserved enzymes and the evolution of novelty in plant specialized metabolism. Plant Physiol **169**: 1512–1523

Møller BL (2010) Functional diversifications of cyanogenic glucosides. Curr Opin Plant Biol **13**: 338–47

Oldroyd GED (2013) Speak, friend, and enter: signalling systems that promote beneficial symbiotic associations in plants. Nat Rev Microbiol **11**: 252–263

Oldroyd GED, Murray JD, Poole PS, Downie JA (2011) The rules of engagement in the legume-rhizobial symbiosis. Annu Rev Genet **45**: 119–44

de Oliveira MVV, Jin X, Chen X, Griffith D, Batchu S, Maeda HA (2019) Imbalance of tyrosine by modulating TyrA arogenate dehydrogenases impacts growth and development of *Arabidopsis thaliana*. Plant J **97**: 901–922

Pérez Guerra JC, Coussens G, De Keyser A, De Rycke R, De Bodt S, Van De Velde W, Goormachtig S, Holsters M (2010) Comparison of developmental and stress-induced nodule senescence in *Medicago truncatula*. Plant Physiol **152**: 1574–1584

Petersen M (2013) Rosmarinic acid: new aspects. Phytochem Rev **12**: 207–227

Pomar F, Merino F, Barceló AR (2002) *O*-4-Linked coniferyl and sinapyl aldehydes in lignifying cell walls are the main targets of the Wiesner (phloroglucinol-HCl) reaction. Protoplasma **220**: 17–28

Qian Y, Lynch JH, Guo L, Rhodes D, Morgan JA, Dudareva N (2019) Completion of the cytosolic post-chorismate phenylalanine biosynthetic pathway in plants. Nat Commun **10**: 15

Rippert P, Matringe M (2002) Purification and kinetic analysis of the two recombinant arogenate

dehydrogenase isoforms of *Arabidopsis thaliana*. Eur J Biochem **269**: 4753–4761

Rosler J, Krekel F, Amrhein N, Schmid J (1997) Maize Phenylalanine Ammonia-Lyase Has Tyrosine Ammonia-Lyase Activity. Plant Physiol **113**: 175–179

Rubin JL, Jensen RA (1985) Differentially regulated isozymes of 3-deoxy-d-arabino-heptulosonate-7-phosphate synthase from seedlings of *Vigna radiata* [L.] Wilczek. Plant Physiol **79**: 711–718

Rubin JL, Jensen RA (1979) Enzymology of L-tyrosine biosynthesis in mung bean (*Vigna radiata* [L.] Wilczek). Plant Physiol **64**: 727–734

Ruijter JM, Pfaffl MW, Zhao S, Spiess AN, Boggy G, Blom J, Rutledge RG, Sisti D, Lievens A, De Preter K, et al (2013) Evaluation of qPCR curve analysis methods for reliable biomarker discovery: bias, resolution, precision, and implications. Methods **59**: 32–46

Schenck CA, Chen S, Siehl DL, Maeda HA (2015) Non-plastidic, tyrosine-insensitive prephenate dehydrogenases from legumes. Nat Chem Biol **11**: 52–57

Schenck CA, Holland CK, Schneider MR, Men Y, Lee SG, Jez JM, Maeda HA (2017a) Molecular basis of the evolution of alternative tyrosine biosynthetic routes in plants. Nat Chem Biol **13**: 1029–1035

Schenck CA, Men Y, Maeda HA (2017b) Conserved molecular mechanism of TyrA dehydrogenase substrate specificity underlying alternative tyrosine biosynthetic pathways in plants and microbes. Front Mol Biosci. doi: 10.3389/fmolb.2017.00073

Schenck CA, Maeda HA (2018) Tyrosine biosynthesis, metabolism, and catabolism in plants. Phytochemistry **149**: 82–102

Seabra AR, Pereira P a, Becker JD, Carvalho HG (2012) Inhibition of glutamine synthetase by phosphinothricin leads to transcriptome reprograming in root nodules of *Medicago truncatula*. Mol Plant Microbe Interact **25**: 976–92

Siehl D (1999) The biosynthesis of tryptophan, tyrosine, and phenylalanine from chorismate. *In* B Singh, ed, Plant Amino Acids Biochem. Biotechnol. CRC Press, New York, pp 171–204

Siehl DL, Tao Y, Albert H, Dong Y, Heckert M, Madrigal A, Lincoln-Cabatu B, Lu J, Fenwick T, Bermudez E, et al (2014) Broad 4-hydroxyphenylpyruvate dioxygenase inhibitor herbicide

tolerance in soybean with an optimized enzyme and expression cassette. Plant Physiol. doi: 10.1104/pp.114.247205

Stacey MG, Cahoon RE, Nguyen HT, Cui Y, Sato S, Nguyen CT, Phoka N, Clark KM, Liang Y, Forrester J, et al (2016) Identification of homogentisate dioxygenase as a target for vitamin E biofortification in oilseeds. Plant Physiol **172**: 1506–1518

Starker CG, Parra-Colmenares AL, Smith L, Mitra RM, Long SR (2006) Nitrogen fixation mutants of *Medicago truncatula* fail to support plant and bacterial symbiotic gene expression. Plant Physiol **140**: 671–680

Strack D, Vogt T, Schliemann W (2003) Recent advances in betalain research. Phytochemistry **62**: 247–69

Streeter J, Wong PP (1988) Inhibition of legume nodule formation and N2 fixation by nitrate. Crit Rev Plant Sci **7**: 1–23

Tadege M, Wen J, He J, Tu H, Kwak Y, Eschstruth A, Cayrel A, Endre G, Zhao PX, Chabaud M, et al (2008) Large-scale insertional mutagenesis using the *Tnt1* retrotransposon in the model legume *Medicago truncatula*. Plant J Cell Mol Biol **54**: 335–47

Tzin V, Galili G (2010) New insights into the shikimate and aromatic amino acids biosynthesis pathways in plants. Mol Plant **3**: 956–72

Van de Velde W, Guerra JCP, De Keyser A, De Rycke R, Rombauts S, Maunoury N, Mergaert P, Kondorosi E, Holsters M, Goormachtig S (2006) Aging in legume symbiosis. A molecular view on nodule senescence in *Medicago truncatula*. Plant Physiol **141**: 711–720

Wang M, Toda K, Block A, Maeda HA (2019) TAT1 and TAT2 tyrosine aminotransferases have both distinct and shared functions in tyrosine metabolism and degradation in *Arabidopsis thaliana*. J Biol Chem **294**: 3563–3576

Wang M, Toda K, Maeda HA (2016) Biochemical properties and subcellular localization of tyrosine aminotransferases in *Arabidopsis thaliana*. Phytochemistry **132**: 16–25

Weng J-K, Philippe RN, Noel JP (2012) The rise of chemodiversity in plants. Science **336**: 1667–1670

Westfall CS, Xu A, Jez JM (2014) Structural evolution of differential amino acid effector regulation in plant chorismate mutases. J Biol Chem **289**: 28619–28628

Wych RD, Rains DW (1978) Simultaneous measurement of nitrogen fixation estimated by acetylene-ethylene assay and nitrate absorption by soybeans. Plant Physiol **62**: 443–448

Xi J, Chen Y, Nakashima J, Wang S, Chen R (2013) *Medicago truncatula esn1* defines a genetic locus involved in nodule senescence and symbiotic nitrogen fixation. Mol Plant Microbe Interact **26**: 893–902

Xing A, Last RL (2017) A regulatory hierarchy of the Arabidopsis branched-chain amino acid metabolic network. Plant Cell **29**: 1480–1499

Yoo H, Widhalm JR, Qian Y, Maeda H, Cooper BR, Jannasch AS, Gonda I, Lewinsohn E, Rhodes D, Dudareva N (2013) An alternative pathway contributes to phenylalanine biosynthesis in plants via a cytosolic tyrosine:phenylpyruvate aminotransferase. Nat Commun **4**: 1–11

Zhao J, Williams CC, Last RL (1998) Induction of Arabidopsis tryptophan pathway enzymes and camalexin by amino acid starvation, oxidative stress, and an abiotic elicitor. Plant Cell **10**: 359–370

MATERIALS AND METHODS:

Plant Materials and Growth Conditions

Medicago truncatula seeds were scarified in concentrated hydrochloric acid for eight minutes and repeatedly washed with water. Seeds were then surface sterilized with bleach for 1.5 minutes followed by repeated water washes. Seeds were placed in sterile water for 16 hours at 4°C and then transferred to germination media (0.5x MS media, 0.8% agar, 1 μM GA_3, pH 7.6), wrapped in aluminum foil and placed at 4°C. After 48 hours plates with sterilized seeds were moved to 22°C. After 24 hours the aluminum foil was removed and the germinated seedings were transferred to standard potting soil and placed in a growth chamber (Conviron). Pots were watered with 1x Hoaglands solution when dry, and grown under 12 hour light:dark cycles with 200 μE light intensity and ~60% humidity.

Genotyping

A single young leaf from 6-week-old plants was placed in 1.7 mL microcentrifuge tube with 600 μL of DNA extraction buffer (10 mM Tris-HCl pH 8.0, 25 mM ethylenediaminetetraacetic acid (EDTA), and 0.5% SDS), pulverized with a mini blue pestle, and incubated at 55°C for 15 minutes. The solution was cooled to room temperature and 200 μL of 5 M ammonium acetate was added, vortexed for 20 seconds and centrifuged at 14,000 g for 3 minutes. The supernatant was transferred to a fresh tube and 600 μL of isopropanol was added, followed by centrifugation

742 at 14,000 g for 1 minute. The supernatant was decanted and the pellet washed with 400 µL of
743 70% ethanol followed by centrifugation at 14,000 g for 1 minute. The supernatant was decanted
744 and the pellet dried for 1 hour in a sterile hood. The resulting DNA was dissovled in 50 µL of
745 H_20. Genotyping PCR reactions contained 1 µM gene and insertion specific primers
746 (**Supplementary Table 2**), 1x EconoTaq PLUS master mix (Lucigen), and genomic DNA. DNA
747 was amplified in a thermocycler with the following conditions: an initial denaturation at 95°C for
748 5 min, 35 cycles of amplification at 95°C for 20 s, 60–65°C for 20 s, 72°C for 60 s, with a final
749 extension at 72°C for 5 min.

750 ***Quantitative reverse transcription PCR (qRT-PCR)***

751 RNA was extracted from leaves of 6-week-old plants. About 50mg of tissue was pulverized in
752 liquid N_2 using a mini pestle. RNA extraction buffer (68mM sodium citrate, 132mM citric acid,
753 1mM EDTA and 2% SDS) was added and vortexed immediately for 10 seconds, the tubes were
754 then placed on their sides for 5 minutes at 22°C. The solution was centrifuged at 12,000g for 2
755 minutes and 400 µL of the supernatant was transferred to a fresh tube. 100 µL of of 1M NaCl was
756 added and mixed by pipetting, followed by addition of 300 µL of chloroform, inverted multiple
757 times and centrifuged at 4°C for 10 minutes at 12,000g. The upper phase was transferred to a new
758 tube and an equal volume of isopropanol was added, mixed by inverting and placed at 4°C for 10
759 minutes. The solution was then centrifuged at 4°C for 10 minutes at 12,000g and the supernatant

760 decanted. The pellet was washed with 70% ethanol, followed by centrifugation for 3 minutes at
761 12,000g and the supernatant decanted and the pellet dried in a sterile hood until all residual
762 ethanol was evaporated. The resulting pellet was redissolved in 25 µL of nuclease free H_20
763 (Promega). To remove DNA, the RNA solution was treated with DNase (Turbo DNase, Fisher)
764 following the manufacturer's protocol. The remaining RNA was quantified using a nano-drop
765 spectrophotometer (Thermo) and diluted to a 20 ng/µL concentration. RNA was converted into
766 cDNA using reverse transcriptase (Applied biosystems) with an oligo d(T) primer.

767 For qPCR, cDNA was diluted to 5 ng/µL and additional 5-fold dilutions were made to
768 calculate primer efficiency. All primer pair efficiencies were between 90-100%. cDNA was
769 mixed with GoTaq qPCR master mix (Promega) containing SYBR green and 300 nM of each
770 primer. Reactions were placed in an Stratagene Mx3000P (Agilent) thermocycler using the
771 following PCR cycle an initial denaturation at 95°C for 10 min, 45 cycles of amplification at
772 95°C for 15 s, 60°C for 30 s, 72°C for 30 s.

773 For relative quantification, Ct values were extracted for each reaction and used to
774 quantify initial cDNA concentration using $2^{-\Delta\Delta C(t)}$ method normalized to a housekeeping gene
775 (*MtPI4K* Kryvoruchko et al., 2016, **Supplementary Table 2**) using the LinRegPCR program
776 (Ruijter et al., 2013). For absolute quantification, pET28a vectors carrying *MtPDH1*, *MtncADH*
777 and *MtADH* were used as the template to amplify a fragment of the corresponding genes. The

778 resulting fragments were purified from 0.8% agarose gels using a QIAquick gel extraction kit
779 (Qiagen) following manufacturer's protocol. The DNA concentration was quantified and repeated
780 5-fold dilutions were made and used to obtain a standard curve in qRT-PCR with gene-specific
781 primers (**Supplementary Table 2**). Ct values were extracted for each qRT-PCR reaction and used
782 to quantify initial cDNA concentration by using the linear range created as above for the
783 respective gene.

784 ***Enzyme extraction and ADH and PDH assays***

785 Leaf tissue from 6-week-old plants were ground to a fine powder in a prechilled mortar and
786 pestle under liquid N_2. Extraction buffer (25 mM HEPES, pH 7, 50 mM KCl, 10% ethylene
787 glycol, 1% polyvinylpyrrolidone (PVP) and 1 mM dithiothreitol (DTT)) was added in a 1:3 ratio
788 of tissue to buffer (w/v). The slurry was centrifuged for 20 min at 4°C, at 20,000 g and the
789 resulting supernatant desalted using a gel filtration column (Sephadex G50-80 resin,
790 Sigma-Aldrich) equilibrated with extraction buffer without DTT and PVP. Protein concentrations
791 were determined by a Bradford assay (Bio-Rad Protein Assay, Bio-Rad).

792 The desalted crude enzyme extracts were used in ADH and PDH reactions that
793 contained 25 mM HEPES (pH 7.5), 50 mM KCl, 10% ethylene glycol, 1 mM $NADP^+$, 1 mM
794 substrate (L-arogenate or prephenate, respectively). Arogenate was prepared by enzymatic
795 conversion from prephenate (Sigma-Aldrich), as previously reported (Maeda et al., 2011).

Reactions were initiated by addition of enzyme from various sources and incubated at 37°C for 45 minutes. The resulting assays were injected into HPLC equipped with a ZORBAX SB-C18 column (Agilent) to directly detect the final product of the assay as described previously (Schenck et al., 2015).

For PDH and ADH activities from various legumes (**Supplementary Fig. 9**), leaf material was obtained from the University of Wisconsin-Madison Botany Department greenhouse or from identified trees on campus. Plants were grown under varying light and temperature conditions and leaf material was collected at different developmental stages. Enzyme extractions and ADH and PDH assays were performed as described above.

Metabolite extraction and detection

Tissue from 6-week-old plants was added into 1.7 mL microcentrifuge tubes with 400 µL of extraction buffer (2:1 (v/v) methanol:chloroform, 0.01 % butylated hydroxytoluene (BHT), 100 µM norvaline and 1.25 µg/mL tocol as previously described (Collakova and DellaPenna, 2003), with 3 glass beads (3 mm). Samples were vigorously shaken for 3 minutes at 1000 r.p.m. using a genogrinder (MiniG 1600, SPEX SamplePrep). Additional chloroform (125 µL) and water (300 µL) were added and vortexed for 30 seconds. Samples were centrifuged for 10 minutes at 20,000 rpm and the polar and non-polar phases were transferred to new tubes and dried using a vacuum concentrator (Labconco).

814 For tocopherol analysis, the dried nonpolar phase was resuspended in methanol with
815 0.01% BHT. Samples were injected into a HPLC (Agilent 1260) equipped with a ZORBAX
816 SB-C18 column (Agilent) using a 30 minute isocratic elution of 95 % methanol, 5 % water.
817 Tocopherols in the extractions were visualized using fluorescence detection excitation at 290 nm
818 and emission at 330 nm and compared with authentic standards (Sigma) and normalized to an
819 internal control (tocol).

820 For anthocyanin detection, 1 M HCl of methanol was added to the polar phase in a 1:1
821 ratio. A spectrophotometer was used to measure absorbance at 520 nm. Absolute levels were
822 estimated using an extinction coefficient of anthocyanin absorbance (Lee et al., 2005) of 33,000
823 $L \times M^{-1} \times cm^{-1}$.

824 The polar and non-polar phases were analyzed with GC-MS. The dried polar phase was
825 redissolved in pyridine with 15.0 mg/mL methoxyamine-HCl. Samples were vortexed for 30
826 seconds followed by sonication for 10 minutes and incubated for 60 minutes at 60°C. This was
827 repeated once more, then the samples were derivatized with an equal volume of
828 *N*-methyl-*N*-(tert-butyldimethylsilyl)trifluoroacetamide + 0.1 % *tert*-butyldimethylchlorosilane
829 (MTBSTFA + 0.01 % t-BDMCS, Sigma-Aldrich) and incubated for 60 minutes at 60°C. Samples
830 were then injected into GC-MS (Trace 1310, ISQ LT, Thermo Scientific). The dried non-polar
831 phase was redissolved in 800 µL of chloroform with 50 ppm BHT and 500 µL of 1.25M HCl in

832 methanol. Following incubation at 50°C for 4 hours, samples were completely dried under
833 nitrogen gas. The dried non-polar phase was resuspended in 70 µL of pyridine and derivatized
834 with 30 µL of MTBSTFA + 0.01 % t-BDMCS (Sigma-Aldrich). Following transfer to a glass
835 vial, 1 µL of the polar and non-polar phases were injected onto a 30 m column (TG-5MS,
836 Thermo Scientific) using a 10:1 split ratio, and an oven ramp method of 5°C per minute for 46
837 minutes and held at 300°C for 10 minutes. Detected compounds were compared with library
838 matches from NIST and peak areas based on ion abundance were normalized to an internal
839 standard (norvaline).

840 ***Acetylene reduction assay (ARA)***

841 Plants used for ARA were scarified and germinated as described previously. Seedlings were
842 transferred to 12” square plates containing modified solid Fahräeus medium supplemented with
843 0.5 mM NH_4NO_3 (Catoira et al., 2000). Plates were grown under the same conditions as pot
844 grown plants, however plates were placed at a ~60° angle so that the roots would not penetrate
845 the agar. After 5 days of growth on plates, each plant was inoculated with 1 mL of water
846 containing *Sinorhizobium meliloti* Rm1021 at an OD_{600} 0.02. Plants were then allowed to grow
847 for 14, 21 and 28 dpi at which point nodules were counted and plants were moved to 10 mL glass
848 jars with 1 mL of sterile water at the bottom. Glass jars were sealed with a rubber stopper, then
849 injected with 1 mL of acetylene gas (10% acetylene final). After 48 hours of incubation at 37°C,

1 mL of the gas from the glass jars was injected into a gas chromatograph (GC-2010, Shimadzu) to measure the production of ethylene and and ARA activity was calculated as described in Hardy et al., 1968.

Histochemical staining of lignin composition

For cell wall composition staining, thin cross sections of stem tissue from 6-week-old plants were prepared using a razor blade. For Mäule staining stem sections were placed in a 1% potassium permanganate solution for 5 minutes, then rinsed with water followed by addition of a 12% HCl (V/V) for 5 minutes and rinsed again with water. A 1.5% solution of sodium bicarbonate was added to facilitate a color change to dark red and visualized using an epifluorescence microscope (Olympus BX60).

For phloroglucinol staining, similar stem cross sections were placed in a well plate with 1 mL of 10 % phloroglucinol (w/v) solution in 95 % ethanol with 500 µL of 10 N HCl and incubated for 5 minutes. Stem sections were transferred to a glass slide and washed with water and visualized using a epifluorescence microscope (Olympus BX60).

GUS staining was performed on nodules developed after inoculation with *S. meliloti* Rm1021 carrying a P*nifH*::*UidA* fusion, to localize expression of the bacterial *nifH* gene, which is required for nitrogen fixation. Nodules were embedded in 4% agarose and 50-100 µM sections were made with a vibratome® 1000 plus (Leica). Sections were immersed in a staining solution

(2.5% 5-Bromo-4-chloro-3-indoxyl-beta-D-glucuronic (X-Gluc), 0.2M sodium phosphate buffer (pH 7), 0.1 M potassium ferricyanide, 0.1 M potassium ferrocyanide, 0.25 M Na_2EDTA, and 10% Triton X-100) and vacuum infiltrated for 10 minutes, incubated in the dark at 37°C for 30 minutes, and rinsed with phosphate buffer. Sections were visualized using bright field microscopy.

SUPPLEMENTARY RESULTS:

Supplementary Table 1. Non-targeted metabolite analysis from leaf tissue of Wt and *mtpdh1-1*

Metabolite	retention time (min)	Ion (m/z)	pdh1-1/ R108	pdh1-2/R108	T-test pdh1-1: R108	T-test pdh1-2:R108
Beta-Alanine	21.5809	248.1	NS	1.49638	NS	0.04629
beta-D-glucoside	32.1517	204.1	1.18350	2.20999	0.01116	0.00016
Citric Acid	30.5877	273.1	NS	1.51560	NS	0.00027
D-(+)-Melibiose	43.5201	204.1	0.72128	NS	0.03323	NS
Ferulic Acid	36.1830	338.2	NS	0.51230	NS	0.01121
Gentisic Acid	29.4116	355.2	NS	2.85714	NS	0.00001
Glucuronic Acid	29.1234	292.2	NS	1.58440	NS	0.00001
Glycolic Acid	11.8422	205.1	1.42874	1.92904	0.01487	0.00037
L-Alanine	19.8168	188.1	NS	2.39806	NS	0.00005
Lauryl Alcohol	22.0027	243.1	1.27167	NS	0.01445	NS
Maleic Acid	18.2630	2455.0	NS	0.68722	NS	0.04895
Malic Acid	23.0106	233.1	NS	0.73291	NS	0.04836
Malonic Acid	15.4680	233.1	0.75424	NS	0.02370	NS
Pinitol	30.8088	260.2	1.33875	NS	0.01147	NS
Propionic Acid	18.8585	292.2	NS	2.08458	NS	0.01253
Saccharic Acid	35.0341	333.2	0.74697	1.32846	0.00476	0.00815
Sucrose	44.9165	361.2	NS	1.99803	NS	0.02979
Tartaric Acid	25.6516	305.2	1.43056	NS	0.03744	NS
Trehalose	43.9602	361.2	NS	18.99309	NS	0.00048
Tyramine	32.7431	174.1	NS	0.59383	NS	0.00075
Unknown	33.6590	204.1	1.26433	NS	0.00363	NS
Unknown	17.5759	186.0	1.79713	2.62694	0.00452	0.01497
Unknown	13.6890	220.1	1.41853	NS	0.00884	NS
Unknown	30.8657	217.1	1.32711	NS	0.00953	NS
Unknown	9.2975	184.1	1.52453	NS	0.01137	NS
Unknown	47.8363	204.2	1.43690	1.35843	0.01504	0.04118
Unknown	47.2028	204.1	1.21975	1.20442	0.03006	0.04871
Unknown	32.5721	221.2	1.21109	NS	0.03112	NS
Unknown	49.3385	217.1	1.31458	1.40117	0.03151	0.01702
Unknown	36.3824	434.3	0.70531	NS	0.03570	NS
Unknown	21.0322	189.1	1.20140	NS	0.04070	NS
Unknown	23.6949	217.1	NS	3.31769	NS	0.00007
Unknown	32.7980	205.1	NS	3.21406	NS	0.00002
Unknown	27.4875	422.2	NS	3.08602	NS	0.01943
Unknown	17.5759	186.0	NS	2.48604	NS	0.01419
Unknown	24.6017	217.1	NS	2.38962	NS	0.00001
Unknown	22.0509	307.2	NS	2.33226	NS	0.00220
Unknown	19.1101	184.1	NS	2.02055	NS	0.04568
Unknown	30.6073	150.1	NS	1.50572	NS	0.00020

Unknown	24.9767	313.3	NS	1.43477	NS	0.04725
Unknown	31.7135	275.2	NS	1.31801	NS	0.00069
Unknown	38.4361	331.1	NS	1.27114	NS	0.00650
Unknown	33.7685	270.2	NS	0.76019	NS	0.03895
Unknown	41.0710	274.1	NS	0.70608	NS	0.01860
Unknown	37.2316	204.1	NS	0.67959	NS	0.02484
Unknown	25.7858	331.2	NS	0.65537	NS	0.01841
Unknown	31.0367	292.2	NS	0.54155	NS	0.00025
Xylose	26.8968	160.1	NS	0.60672	NS	0.00493

Only compounds are shown that were significantly different from Wt with abundance > 1.2 or < 0.8 fold-change and a P-value ≤ 0.05. Ratio of average relative metabolite abundance is shown for *pdh1-1* and *pdh1-2* compared with Wt with N = 5. NS, not significant. Unknowns are compounds that were detected with unique ions, but did not have a confident library match (< 75%).

Supplementary Table 2. Primer sequences used in this study.

Name	Use	Sequence (5'-3')
PDH1-1	*mtpdh1-1* genotyping	GAGCACTATTTCCATTGTTAAC
Tnt1R	*mtpdh1-1* genotyping	CAGTGAACGAGCAGAACCTG
PDH1-2	*mtpdh1-2* genotyping	ATGAGACTGGAGGGGGAGAT
Tnt1F	*mtpdh1-1* genotyping	GAACATATGGCAGGGGTTACAAG
MtPDHqF1	*mtpdh1-1* qPCR	AAACAAGGTCATACTCTAACTGCAA
MtPDHqR1	*mtpdh1-1* qPCR	CAGCATCAAGGAATGCTGTAA
MtPDHqF2	*mtpdh1-2* qPCR	CAACAGATTCGCCAGACAAGAGC
MtPDHqR2	*mtpdh1-2* qPCR	CTGGGTTCTGTCCTTCATCGA
MtADHqF	*MtADH* (Medtr4g115980) qPCR	GACCTGAGAGTGGAAGCAGT
MtADHqR	*MtADH* (Medtr4g115980) qPCR	TTCTCACACCTCGAAACCCT
MtncADHqF	*MtncADH*(Medtr5g083530) qPCR	GCTAGTGAGGGTTGTAAGATGC
MtncADHqR	*MtncADH*(Medtr5g083530) qPCR	GCGGGTAATTCTGTATTATT
MtPI4KF[1]	housekeeping gene (*MtPI4K) qPCR*	GCAGATAGACACGCTGGGA
MtPI4KR[1]	housekeeping gene (*MtPI4K) qPCR*	AACTCTTGGGCAGGCAATAA
MtHPPD1F	*MtHPPD1* (Medtr5g091060) qPCR	CCCACCAACACCACTTCTCT
MtHPPD1R	*MtHPPD1* (Medtr5g091060) qPCR	GGTGCTGGGTTACAGCATTT
MtHGOF	*MtHGO* (Medtr8g463280) qPCR	AGGCACGGGTTCCTTCTAAT
MtHGOR	*MtHGO* (Medtr8g463280) qPCR	TCAATGAAATCCGTTGGTGA
MtMAAIF	*MtMAAI* (Medtr4g134370) qPCR	CTTCCATGGGTCCAGAGTGT
MtMAAIR	*MtMAAI* (Medtr4g134370) qPCR	CCGCCATGAAAACTTCATCT
MtFAHF	*MtFAH* (Medtr2g025640) qPCR	ACTTCGGACCCACATTGAAG
MtFAHR	*MtFAH* (Medtr2g025640) qPCR	TCCACAGGTTTTCCCAGTTC
MtVPEF[2]	*MtVPE* (Medtr1g016780) qPCR	AGTTCTGCCTGTTGTGGAATGTC
MtVPER[2]	*MtVPE* (Medtr1g016780) qPCR	GGTAGCTCCTGTCTGCCAATTAC

[1] Housekeeping gene (Kryvoruchko et al., 2016) used in normalization of qPCR data.

[2] Cysteine protease (vacuolar processing enzyme; VPE) that serves as a senescence marker gene (Pérez Guerra et al., 2010).